Evidence for a Pressure-Driven Instability in the CTX Spheromak

F. J. Wysocki, J. C. Fernández, I. Henins, T. R. Jarboe, and G. J. Marklin
Los Alamos National Laboratory, Los Alamos, New Mexico 87545
(Received 12 September 1988)

Recent improvements in the operation of the CTX spheromak device have produced discharges containing evidence for a pressure-driven instability. The instability leads to a distinct event in the discharge, which can be studied in detail. Data are presented which reasonably discount Taylor relaxation of the current profile as the cause of the event. The critical value of the normalized pressure gradient has been measured and is compared with the Mercier limit.

PACS numbers: 52.55.Hc, 52.35.Py

A spheromak[1] is a toroidal magnetic configuration with large toroidal and poloidal plasma currents which generate most of the internal magnetic field. This configuration is attractive for a fusion reactor because it is compact, has a high level of Ohmic heating power, and thus, may not require auxiliary heating (such as neutral beam or rf injection), and has a high engineering β ($\beta_{\rm eng} \propto P/B_{\rm wall}^2$). However, the theoretically predicted internal β ($\beta_{\rm vol} \propto P/\langle B^2\rangle_{\rm vol}$) calculated with the Mercier criterion is small, ranging from $\approx 0.2\%$ for the "classical" spheromak[1] to (1–2)% for nonspherical cross sections,[1–3] to $\gtrsim 7\%$ for the spheromaks with current holes.[2–4] In fact, many other toroidal magnetic configurations have low predicted β limits. Tokamaks are theoretically limited by the ballooning criterion[5] to $\lesssim$(5–10)%, and reversed field pinch equilibria stable to current-driven resistive tearing modes have a predicted β limit[6] of $\approx 20\%$. The experimental significance of predicted β limits is often unclear, since other effects might limit plasma performance. If the β limits could be reached, the expected plasma behavior is often unknown. Tokamaks historically have had difficulty reaching the predicted β limit,[5] but recently large tokamaks have been used to explore plasma conditions at reactor relevant β values. The highest values obtained are empirically found to follow a scaling law of the form $\beta_{\rm max} \approx 3I/aB$ (in %, MA, m, and T)[7,8]; however, this can be consistent with either ballooning mode or kink mode limits.[7] In addition, operation at this β limit is found to be disruptive[7] in some cases and in other cases a degradation of energy confinement without disruption is observed.[8] Reversed field pinches normally operate[6] with roughly constant β ($\approx 10\%$), indicating an empirical limit, but the value is less than the predicted value, which does not include the localized resistive interchange mode (sometimes called the "g mode"). In contrast, spheromaks often have β values above those predicted.[9,10]

In this Letter, strong evidence for a pressure-driven instability in CTX[11] spheromaks is presented. The instability leads to a distinct event in the discharge which can be analyzed in detail. It is found that when a particular threshold value in the pressure gradient is exceeded, internal plasma is expelled toward the wall in 10–20 μs. The resulting temperature and density profiles are both hollow (about the magnetic axis), strongly indicating a magnetic flux interchange. These hollow profiles are short lived, and evolve back to moderately peaked profiles in 30–60 μs. The magnetic field probe data indicate that the instability is not Taylor relaxation[12] of the current profile.

Several recent changes in the operation of the CTX spheromak device were necessary to obtain plasma conditions that lead to clear evidence of the instability. These changes include replacement of the mesh-wall flux conserver[13] (0.67-m radius) with a solid-wall flux conserver (simple cylinder with 0.61-m radius and 0.62-m long), resulting in greatly reduced magnetic field errors. Titanium gettering is used to obtain clean discharges.[14] A small amount of bias field[13] is applied (the bias flux inside the 0.61-m radius of the flux conserver midplane is $\lesssim 5\%$ of the spheromak poloidal flux), which was empirically found to increase the number of high-quality discharges obtainable (>25) before regettering was necessary. Under these conditions, the particle and energy confinement times are substantially higher (up to a factor of ≈ 4) than those achieved in the mesh flux conserver.[15]

The CTX diagnostics include an array of 32 wall poloidal magnetic field probes used to determine both the magnetic equilibrium and any current-driven modal activity,[16] multipoint Thomson scattering absolutely calibrated for density with Raman scattering, and an eight chord CO_2 interferometer with impact parameters (b) measured from the geometric symmetry axis ranging from 0 to 0.54 m.

Figure 1(a) shows the typical time evolution of the toroidal plasma current, and both the central ($b=0.32$ m) and edge ($b=0.54$ m) line-averaged electron density ($\langle n_e\rangle_{\rm line}$). Magnetic helicity[12] and plasma were injected from the gun[11] until 0.7 ms. Since the gun is magnetically connected to the edge of the spheromak, the injected plasma maintains the high-edge electron density during sustainment. While the plasma density profile is

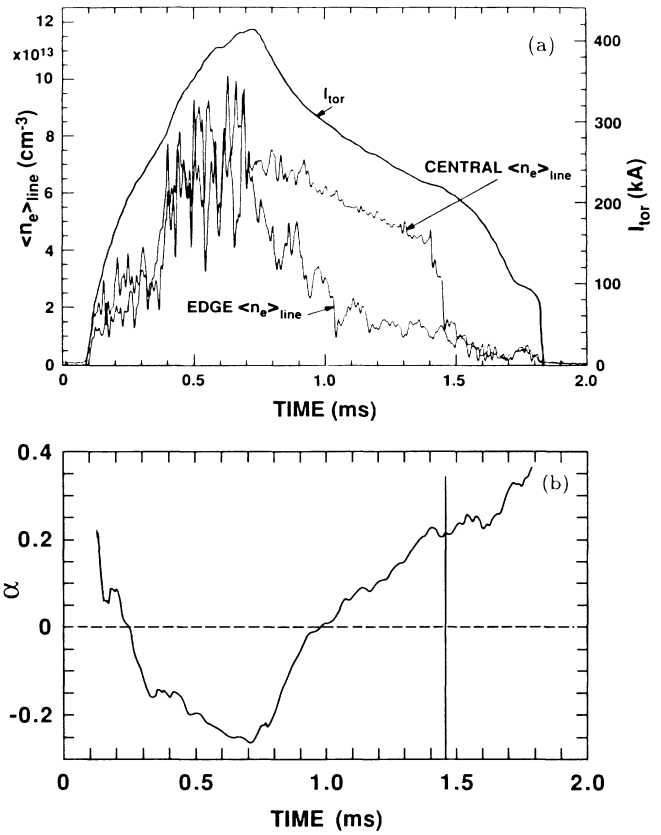

FIG. 1. A typical CTX discharge with a pressure-driven instability. (a) Toroidal plasma current as inferred from the B_{wall} data, and the central-beam ($b=0.32$ m) and edge-beam ($b=0.54$ m) interferometer data and (b) the current peaking parameter (α), which is defined in the text. The slight variation in α just before the instability is insignificant because of the following: (1) It is no larger than other random variations in the trace and (2) the linear $\lambda(\psi)$, zero β model is not accurate to that precision.

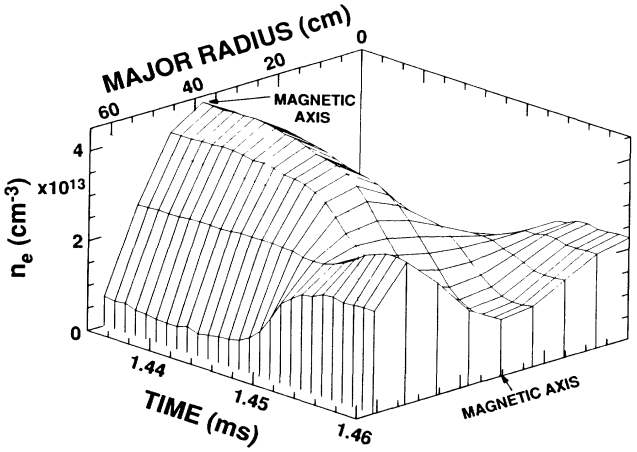

FIG. 2. Electron density profile inferred from unfolding the eight-beam interferometer data from the discharge shown in Fig. 1 for times near the pressure-driven instability.

roughly flat during this time, structure in the profile is indicated by the fluctuations in $\langle n_e \rangle_{line}$ due to the rotating $n=1$ kink mode[15] normally present during sustainment.[16] After helicity and plasma injection stop, the plasma current resistively decays, and without the main source of edge plasma density, the edge $\langle n_e \rangle_{line}$ drops. The oscillations (with a period of ≈ 0.12 ms) in the edge $\langle n_e \rangle_{line}$ are due to the rotating $n=2$ kink mode normally present during decay.[16] The central $\langle n_e \rangle_{line}$ remains high until ≈ 1.45 ms, at which time there is a sudden and dramatic loss of central density. The eight-beam interferometer data can be unfolded to give the electron density profile as a function of major radius, as shown in Fig. 2 for times near the loss of central density. Notice that the electron density is strongly peaked about the magnetic axis just prior to the instability, and becomes hollow about the magnetic axis in less than 20 μs. At this time, the plasma current is still high and shows no signature of the instability. The rapid decay of plasma current starting ≈ 0.1 ms after the instability is due to the substantially reduced plasma density. Rapid current decay associated with reduced density may be due to either a streaming instability or electron-neutral collision dominated resistance in the edge region.[15] If the pressure-driven instability reduces the central density less severely, the discharge continues until a subsequent instability occurs, which corresponds to a repeaking of the pressure profile until the instability threshold is again attained. In many discharges the instability occurs 2–3 times.

The sudden loss of central density does not appear to be related to Taylor current-profile relaxation,[12] unlike the "stepwise instability" reported by the CTCC-I spheromak group.[14] The B_{wall} probe data would indicate any changes in the equilibrium[16] associated with current-profile relaxation [i.e., flattening of the $\lambda(\psi) \equiv \mathbf{J}\cdot\mathbf{B}/|B|^2$ profile, where ψ is the poloidal magnetic flux], and it is expected that the probes should also indicate the fluctuation magnetic field associated with the current-driven modes presumed to cause Taylor current-profile relaxation.[17] In CTCC-I, a definite signature in the B_{wall} signals is associated with the "stepwise instability," and a relaxation towards the Taylor minimum-energy state is observed.[14] In contrast, there is no change in the global $\lambda(\psi)$ profile (i.e., the magnetic configuration does not relax toward the Taylor minimum-energy state during the instability), and there is no obvious fluctuation magnetic signature associated with the sudden loss of central density in CTX discharges.

A way of describing the global λ profile is through the use of the parameter α defined as[16] $\lambda(\psi) = \langle\lambda\rangle[1 + \alpha(2\psi - 1)]$, where $\psi = 1$ at the magnetic axis and zero at the edge. The value of α is determined by a least-squares fit of the B_{wall} probe data to calculated values (zero β equilibria). The typical time evolution of α is

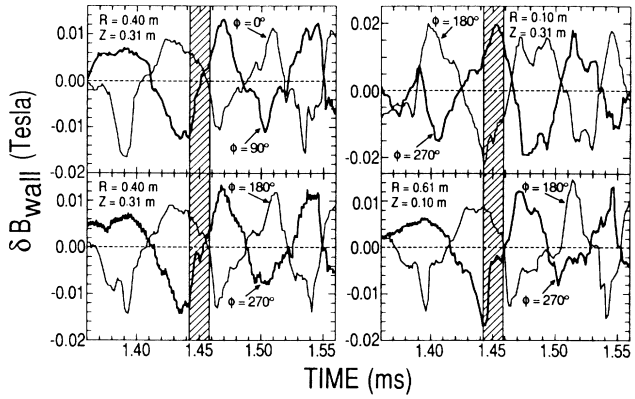

FIG. 3. The fluctuating poloidal B_{wall} data [i.e., $\delta B(t) = B(t) - \langle B \rangle_{0.1\,\text{ms}}(t)$, the average is performed with a square averaging window 0.1 ms wide] from the discharge shown in Fig. 1 for times near the pressure-driven instability (the shaded region indicates the time of the instability). Indicated are the data from four toroidal angles at $R_{\text{major}} = 0.4$ m, $Z = 0.31$ m (measured from the midplane), and at two toroidal angles for positions (0.1 m, 0.31 m) and (0.61 m, 0.1 m). The data not shown from the other two angles are similar.

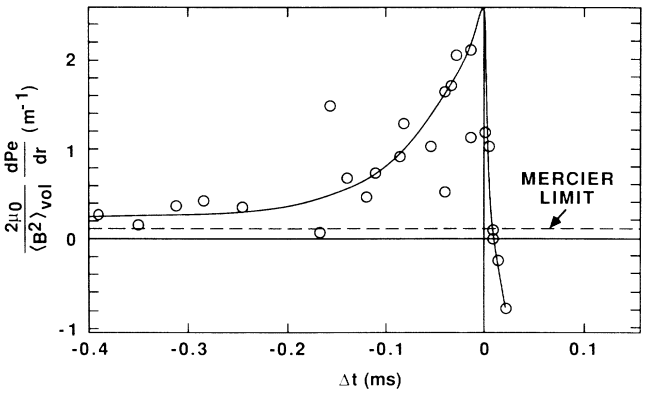

FIG. 4. The maximum electron pressure gradient, as determined from the multipoint Thomson scattering, normalized to $\langle B^2 \rangle_{\text{vol}}$. For hollow profiles, the maximum negative gradient is used. The laser firing time is indexed to the time of the instability (i.e., $\Delta t = t_{\text{laser}} - t_{\text{instability}}$). The dashed line indicates the calculated Mercier limit for $\alpha = 0.25$.

shown in Fig. 1(b). The value of α is less than zero when J/B is peaked toward the edge, and greater than zero when J/B is peaked toward the magnetic axis. The value of α is essentially unchanged by the instability. Current-profile relaxation would make a dramatic change in the value of α as the $\lambda(\psi)$ profile is flattened (i.e., the minimum energy state corresponds to $\alpha = 0$).

Further evidence which indicates that the instability is not current-profile relaxation but is the time behavior of the fluctuations in B_{wall}, as shown in Fig. 3. The oscillations are due to a rotating kink mode with toroidal mode number $n = 2$. At the time of the instability, there is no obvious change in the $n = 2$ oscillations, including amplitude, phase, and rotation speed.

Numerical 3D nonlinear magnetohydrodynamic simulations of decaying spheromaks[17] show distinct relaxation events when the Lundquist number S (ratio of the resistive decay time to the Alfvén transit time) is in the range $400 \lesssim S \lesssim 2000$. The stepwise instability observed in CTCC-I is consistent with this.[14] However, for large S ($\gtrsim 2000$), the simulations indicate that only the 3D quasiequilibria phase would likely to be observed and the spheromak would resistively die out before the final relaxation could occur. This phase is characterized by the presence of a saturated $n = 2$ mode. For discharges like that shown in Fig. 1, S is $\approx 10^4$ (calculated with $S \approx 2\langle\lambda\rangle V_{\text{Alfvén}} \tau_{B^2}$). The fact that the $n = 2$ mode is still present after the loss of central density strongly indicates that current-profile relaxation has not occurred, consistent with the simulation for large S. Thus, based on this critical examination of the B_{wall} probe data, explanation of the sudden loss of central density as Taylor current-profile relaxation is reasonably discounted. The supporting evidence for a pressure-driven instability is now presented.

The multipoint Thomson scattering is used to determine the electron pressure profile, and the laser firing time is indexed to the time of the instability (which may occur anywhere between 0.4 and 1.0 ms after the helicity source is turned off). The magnetic axis temperature is found to increase, from typically ≈ 50 eV at 0.2 ms before the instability, to 100–150 eV at the onset of the instability. During this time, the volume-averaged electron β, $\langle \beta_e \rangle_{\text{vol}} \equiv 2\mu_0 \langle n_e T_e \rangle_{\text{vol}} / \langle B^2 \rangle_{\text{vol}}$, is roughly constant at (1–3)%, but the peak electron β, $\beta_e|_0 \equiv 2\mu_0 (n_e T_e)_0 / \langle B^2 \rangle_{\text{vol}}$ [where $(n_e T_e)_0$ is evaluated at the magnetic axis], increases from typically 5% at 0.2–0.3 ms before the instability to $\approx 20\%$ at the onset of the instability. This is consistent with a strong peaking of the pressure profile as the instability time is approached. Immediately after the instability, $\beta_e|_0 \lesssim 5\%$, but $\langle \beta_e \rangle_{\text{vol}}$ is essentially unchanged, consistent with a flattening of the pressure profile without significant loss of average pressure.

In magnetohydrodynamics, pressure-driven instabilities are driven by normalized pressure gradients ($\nabla P / B^2$), not β (be it peak or volume averaged). Only under the assumption of a profile shape does a pressure gradient limit correspond to a β limit. Since the pressure profile shape is changing in time for these CTX discharges, a more meaningful quantity to consider is the maximum normalized pressure gradient. These data, determined by the multipoint Thomson scattering, are shown in Fig. 4. The electron pressure gradient increases until a threshold value is attained, and then the profile becomes hollow in $\lesssim 20$ μs. Figure 5 shows typical Thomson-scattering pressure profiles just before and just after the instability. Comparison of the two profiles strongly indicates magnetic flux interchange. The lack of a signature on the B_{wall} data indicates that the insta-

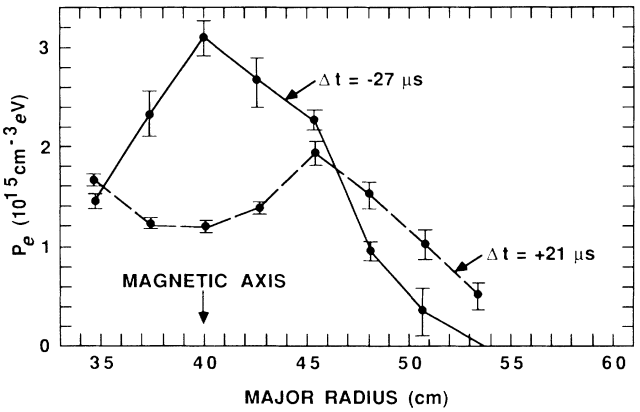

FIG. 5. Typical multipoint Thomson-scattering pressure profiles showing data just before and just after a pressure-driven instability. In the figure, $\Delta t = t_{\text{laser}} - t_{\text{instability}}$.

bility is purely internal, and the flux interchange does not cause flux conversion (i.e., conversion of toroidal flux to poloidal flux, or vice versa). This is consistent with 3D numerical simulations.[18] The good correlation between the onset of the instability and a strongly peaked pressure profile indicates the instability is pressure driven.

The Mercier pressure gradient limit has been calculated for the CTX geometry with $\alpha = 0.25$, which is the approximate average value at the time of the instability. The calculation[4] gives a β_{vol} of 0.4%, and the maximum Mercier pressure gradient is indicated in Fig. 4. The actual electron pressure gradient exceeds this Mercier limit by a factor of ≈ 20. Single-chord O V impurity-ion Doppler-broadening measurements indicate the ion temperature is comparable to T_e. Therefore, the total electron plus ion pressure gradient may exceed the Mercier limit by a factor of ≈ 40. The comparison with theory is still being evaluated. The assumption of linear $\lambda(\psi)$ may not be adequate, and a search for different $\lambda(\psi)$ profiles consistent with the B_{wall} data is ongoing. Calculated equilibria, including the measured $P_e(R)$ profiles, with higher Mercier limits are sought.

The authors acknowledge the expert technical assistance of Robert Bollman, Richard Scarberry, Dennis Martinez, Rita Gribble, and Phillip Klingner. This work was supported by the U.S. DOE.

[1]M. N. Rosenbluth and M. N. Bussac, Nucl. Fusion **19**, 489 (1979).
[2]P. Gautier *et al.*, Nucl. Fusion **21**, 1399 (1981).
[3]S. C. Jardin, Nucl. Fusion **22**, 629 (1982).
[4]R. M. Mayo and G. J. Marklin, Phys. Fluids **31**, 1812 (1982).
[5]J. P. Freidberg, Rev. Mod. Phys. **54**, 801 (1982).
[6]H. A. Bodin *et al.*, Fusion Tech. **10**, 307 (1986).
[7]R. D. Stambugh *et al.*, in *Proceedings of the Tenth International Conference on Plasma Physics and Controlled Nuclear Fusion Research, London, 1984* (IAEA, Vienna, 1985), Vol. 1, p. 217.
[8]G. Becker *et al.*, Nucl. Fusion **27**, 1785 (1987).
[9]G. W. Hart *et al.*, Phys. Rev. Lett. **51**, 1558 (1983).
[10]C. W. Barnes *et al.*, Nucl. Fusion **25**, 1657 (1985).
[11]T. R. Jarboe *et al.*, Phys. Rev. Lett. **51**, 39 (1983).
[12]J. B. Taylor, Phys. Rev. Lett. **33**, 1139 (1974).
[13]C. W. Barnes *et al.*, Phys. Fluids **28**, 3443 (1985).
[14]T. Uyama *et al.*, Nucl. Fusion **27**, 799 (1987).
[15]J. C. Fernández *et al.*, Nucl. Fusion (to be published).
[16]S. O. Knox *et al.*, Phys. Rev. Lett. **56**, 842 (1986).
[17]A. Sgro *et al.*, Phys. Fluids **30**, 3219 (1987).
[18]K. Katayama and M. Katsurai, Phys. Fluids **29**, 1939 (1986).